PCCP

First Principles Modeling of Polymer Encapsulant Degradation in Si Photovoltaic Modules

Journal:	*Physical Chemistry Chemical Physics*
Manuscript ID	CP-ART-02-2021-000665.R1
Article Type:	Paper
Date Submitted by the Author:	11-Apr-2021
Complete List of Authors:	Mannodi Kanakkithodi, Arun Kumar; Argonne National Laboratory, Center for Nanoscale Materials Kumar, Rishi; University of California San Diego Fenning, David; University of California San Diego, Chan, Maria; Argonne National Laboratory, Center for Nanoscale Materials

PCCP

ARTICLE TYPE

Cite this: DOI: 00.0000/xxxxxxxxxx

First Principles Modeling of Polymer Encapsulant Degradation in Si Photovoltaic Modules

Arun Mannodi-Kanakkithodi,*[a] Rishi E. Kumar,[b‡] David P. Fenning,[b‡] and Maria K.Y. Chan[a]

Received Date
Accepted Date

DOI: 00.0000/xxxxxxxxxx

An outstanding issue in the longevity of photovoltaic (PV) modules is the accelerated degradation caused by the presence of moisture. Moisture leads to interfacial instability, de-adhesion, encapsulant decomposition, and contact corrosion. However, experimental characterization of moisture in PV modules is not trivial and its impacts can take years or decades to establish in the field, presenting a major obstacle to designing high-reliability modules. First principles calculations provide an alternative way to study the ingress of water and its detrimental effect on the structure and decomposition of the polymer encapsulant and interfaces between the encapsulant and the semiconductor, the metal contacts, or the dielectric layer. In this work, we use density functional theory (DFT) computations to model single chain, crystalline and cross-linked structures, infrared (IR) signatures, and degradation mechanisms of ethylene vinyl acetate (EVA), the most common polymer encapsulant used in Si PV modules. IR-active modes computed for low energy EVA structures and possible decomposition products match well with reported experiments. The EVA decomposition energy barriers computed using the Nudged Elastic Band (NEB) method show a preference for acetic acid formation as compared to acetaldehyde, are lowered in the presence of a water solvent or hydroxyl ion catalyst, and match well with reported experimental activation energies. This systematic study leads to a clear picture of the hydrolysis-driven decomposition of EVA in terms of energetically favorable mechanisms, possible intermediate structures, and IR signatures of reactants and products.

1 Introduction

Improvements in solar energy technologies are paramount in an age where the world is increasingly moving towards renewable sources of energy to replace fossil fuels and combat climate change. While there is increasing focus on emerging photovoltaic (PV) technologies such as halide perovskites, and maturing thin film technologies such as CdTe and Copper Indium Gallium Selenide (CIGS) are competitive, the vast majority of PV modules produced and in use today are based on crystalline Si. Figure 1(a) shows a general schematic of a Si solar cell module[1] containing different components such as glass sheets, EVA, Si absorber, and metal contact layer(s) such as Cu, Ag or Al[2]. The durability of Si PV modules is determined by the nature of encapsulants, metallic contacts, dielectric layers[3] and various interfaces, as well as by environmental conditions and their effect on different module components. An important issue in Si modules is the increased degradation and detrimental performance caused by the presence of moisture. It has been shown that the ingress of water in Si modules causes loss of adhesion at the interface between ethylene vinyl acetate (EVA), the most common polymer used as solar module encapsulant, and the Si absorber, leading to delamination and degradation[4,5]. Water also leads to an increased likelihood of potential-induced degradation, corrosion at contacts, and the decomposition of EVA, typically in the form of acetic acid loss, or deacetylation.

Despite the danger of water-induced interfacial degradation, the real-time observation and quantification of water in PV modules remains an active area of research, and is currently performed crudely by evaluating general performance degradation where factors other than moisture are certainly playing a role. Recent work shows that the detection of water ingress in PV modules by its IR signature holds promise as a quantitative approach[6]. The molecular mechanisms for water-induced EVA degradation are not fully known. First principles computations provide a means of fundamentally studying the moisture ingress problem and guiding experiments in terms of the influence of water on the structure, IR signatures, surfaces, interfaces and decomposition mechanisms of polymer encapsulants, Si,

[a] Center for Nanoscale Materials, Argonne National Laboratory, Argonne, IL, USA; E-mail: mannodiarun@anl.gov
[b] Department of NanoEngineering, University of California San Diego, CA, USA.
† Electronic Supplementary Information (ESI) available: [details of any supplementary information available should be included here]. See DOI: 10.1039/cXCP00000x/

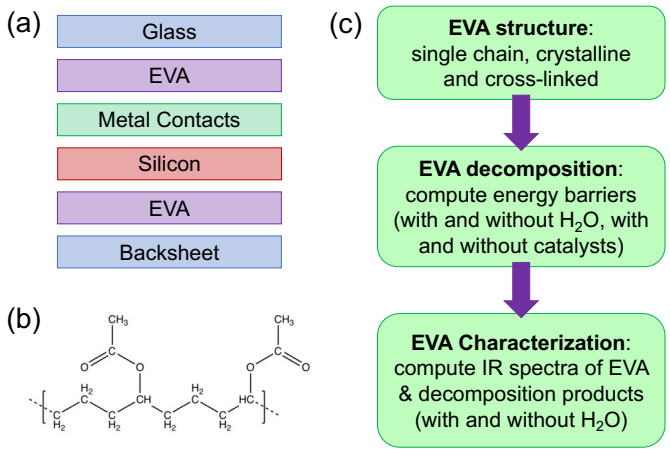

Fig. 1 (a) Schematic of a Si solar cell module, containing components such as the polymer encapsulant (EVA), metal contacts (such as Cu or Ag) and front/back glass sheets. (b) EVA chemical repeat unit used in this work. (c) Outline of the computational work, from EVA structure to decomposition to characterization.

dielectric layers and metallic contacts. Density functional theory (DFT) has been successfully used in the past to model low energy crystalline conformations of organic polymers [7–9], reliably calculate dielectric permittivities and IR active modes [10,11], and simulate realistic cross-linked polymer structures [12–15]. DFT has further proven particularly useful in modeling reaction mechanisms and energy barriers via the Nudged Elastic Band (NEB) method, where transition state structures are generated between reactants and products by nudging each intermediate structure closer to the path of least resistance [16,17].

In this work, we performed DFT computations to study the structures, deacetylation mechanisms and characteristic IR spectra related to EVA, and compared our results with reported experiments wherever possible. The chemical repeat unit of EVA is pictured in Figure 1(b) and the computational outline of this work is presented in Figure 1(c). The EVA molecular structure was simulated as an isolated single chain, in a three-dimensional crystalline arrangement with closely packed chains, and as a cross-linked crystal structure. NEB was applied to model the deacetylation mechanisms of cross-linked EVA, with and without the presence of water and possible catalysts, following the two primarily studied mechanisms from the literature, the Norrish I and Norrish II mechanisms [4,18,19] leading to the formation of acetaldehyde and acetic acid, respectively. IR spectra computed for all EVA structures and decomposition products qualitatively match well with measured vibrational modes corresponding to C=O, O-H or C-H bonds, as collected from the literature for EVA and related materials. NEB computed energy barriers showed that the Norrish II mechanism is preferable to Norrish I, and the barriers are always lower in the presence of a water solvent than in vacuum. It was also seen than NEB barriers went down for a lower percentage of deacetylation, as well as in the presence of a catalyst such as a hydroxyl ion, indicating a hydrolysis-driven enhancement in acetic acid loss and polymer degradation.

In the following sections, we lay out the computational details and present the results on structure modeling, deacetylation reaction mechanisms and barriers, and IR spectra modeling for relevant systems. We finish with a discussion of how this systematic computational study can inform future experiments and create a path towards understanding and eliminating water-induced damages in Si PV modules.

2 Methods

2.1 Computational Details

All calculations were performed using the Vienna ab-initio Simulation Package (VASP) employing the projector-augmented wave (PAW) atom potentials and the van der Waals (vdW)-corrected generalized gradient approximation (GGA) functional vdW-DF2, which explicitly takes vdW dispersion interactions into account that are important for stabilizing soft materials like polymers [10,20]. The kinetic energy cut-off for the planewave basis set was 500 eV, and all atoms were relaxed until forces on each were less than 0.05 eV/Å. Brillouin zone integration was performed using a Monkhorst-Pack mesh density of 0.2 $Å^{-1}$. The low energy crystal structures of EVA and possible decomposition reaction products were obtained for unit cells containing two or four closely packed polymer chains using the minima hopping algorithm [21,22], with all energies determined using DFT. IR spectra of any single chain, crystalline or cross-linked EVA polymer and decomposition products were computed using density functional perturbation theory (DFPT) [10,23]. NEB calculations [16,17] were performed by simulating 5 intermediate structure images between the starting EVA structure and the product polymer, and the same DFT parameters were used as described above. The climbing image method and the limited-memory Broyden-Fletcher-Goldfarb-Shanno optimizer as implemented in VASP was used for NEB [17], with default values used for maximum step size, number of steps, and other parameters. The NEB calculations were performed in vacuum as well as in a continuum solvation environment imposed using the VASPsol code [24], which enables the comparison of decomposition energy barriers in vacuum and in the presence of a solvent.

2.2 Modeling Single Chain, Crystalline and Cross-Linked Structures of EVA and Decomposition Products

We used the molecular structure of EVA with the chemical repeat unit –[CH_2-CH_2-CH_2-CH(-O-CO-CH_3)]– to create the isolated single chain, closely packed crystal structure and crystalline cross-linked structures as shown in Fig. 2. The single chain EVA structure enables the simulation of IR active modes and decomposition reactions in an isolated chain that does not interact with adjoining polymer chains, and is contained in a slab with about 15 Å of vacuum that ensures non-interaction. The single chain structures differ from the closely packed crystalline arrangements in terms of a lack of van der Waals interactions between polymer chains and an enhanced free volume in

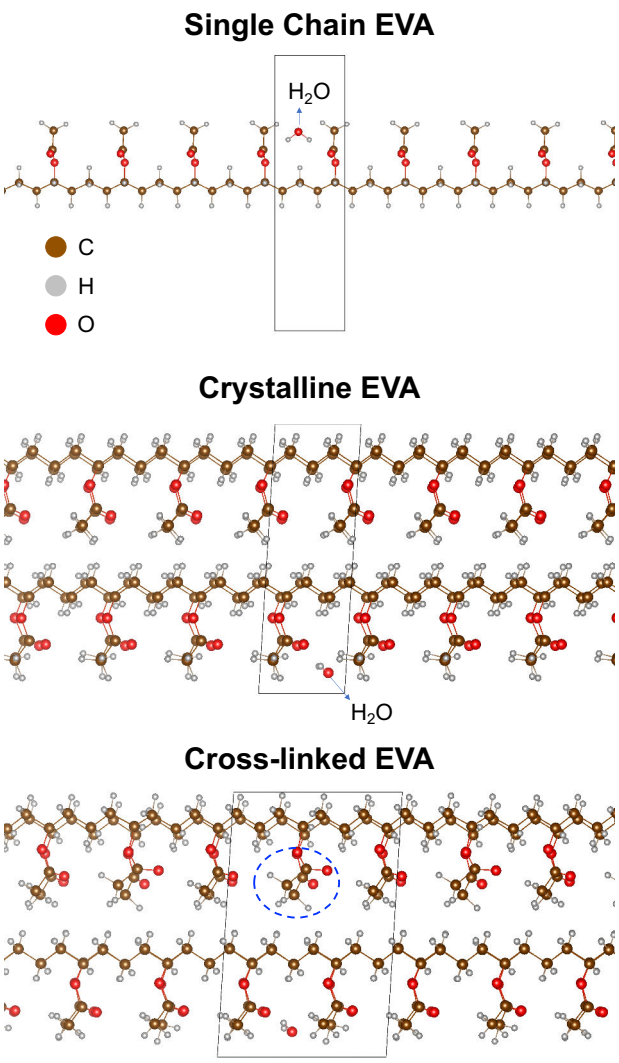

Fig. 2 Single chain, crystalline and cross-linked EVA atomistic structures used for DFT computations in this work.

the system. The crystalline renditions of EVA were simulated following a strategy described in the past for polymer crystal structure prediction[8,9]. We considered a box with 4 closely packed EVA chains repeating indefinitely along the direction of the chain following periodic boundary conditions. Starting from an arbitrary packing arrangement and lattice parameters, the minima hopping algorithm (MHM)[21,22] was applied and the lowest energy structure was obtained, with all energies calculated from DFT using the input parameters described in the Computational Details section. Also pictured in each structure in Fig. 2 is a single H_2O molecule simulated within the polymer unit cell in order to take into account the water related modes when calculating the IR spectra.

Cross-linking in polymers is known to greatly affect their stability, electronic structure and degradation, and consequently their performance as encapsulants in PV modules. We incorporated cross-linking starting from the low energy crystal structure as obtained from MHM, and creating a connection between adjoining polymer chains via the branching acetate (-O-CO-CH_3) units. This cross-linked structure is pictured in Fig. 2 and is used to make comparisons with properties estimated for single chain and crystalline EVA. We apply a cross-linking fraction of 25% while modeling the cross-linked EVA structure, which is similar to fractions generally reported in the experimental literature where solvent extraction is used to determine the amount of cross-linking in terms of the gel content[25,26].

When decomposition of EVA is modeled, the acetate unit is lost and the reaction products are (a) acetaldehyde and a product polymer with a ketone linkage in the backbone, if following the Norrish I mechanism, and (b) acetic acid and a product polymer with a C=C double in the polymer backbone, if following the Norrish II mechanism[4,19]. The reactant (EVA with a double repeating unit structure to illustrate the loss of one acetate unit) and final products for either mechanism are pictured in Fig. 3 in terms of chemical reaction schema. For the product polymers with the repeat units shown in Fig. 3, we once again created single chain, crystalline and cross-linked crystal structures, following the same procedure as described here for EVA. Eventually, characterization in terms of IR spectra was performed for all EVA structures, all product polymer structures, acetaldehyde and acetic acid, and we plot the intensities of various computed IR active modes as a function of wavenumber across all the systems in Fig. 6.

2.3 Nudged Elastic Band Method to Model EVA Deacetylation Mechanisms

The Norrish I and Norrish II mechanisms for deacetylation of EVA are pictured in Fig. 3, highlighting the formula units of the starting structure, the product polymer, the aldehyde or acid product, and the chemical blocks that cleave off from the polymer backbone. It can be seen that in the Norrish I mechanism, the -C(=O)-CH_3 block detaches from the EVA backbone and leaves behind a ketone C=O linkage in the product polymer and acetaldehyde as the byproduct. However, the Norrish II mechanism involves breakage of the entire -O-C(=O)-CH_3 acetate unit, leading to the creation of a C=C double bond in the polymer backbone and an acetic acid byproduct. It should be noted that in much of the literature, acetic acid formation has been observed, which would point towards Norrish II being the more favorable method of EVA decomposition. Other possible EVA degradation mechanisms reported in the literature include the Norrish III mechanism leading to the formation of a ketone and aldehyde, and a photodegradation process leading to the formation of lactone and methane[4]; we focus on Norrish I and Norrish II mechanisms in this work because of their comparatively favorable energetics.

In order to model in detail Norrish I and Norrish II mechanisms, we used a pseudo-isolated single chain version of cross-linked EVA. The bottom half of the cross-linked structure shown in Fig. 2 was removed and the vacuum in the slab

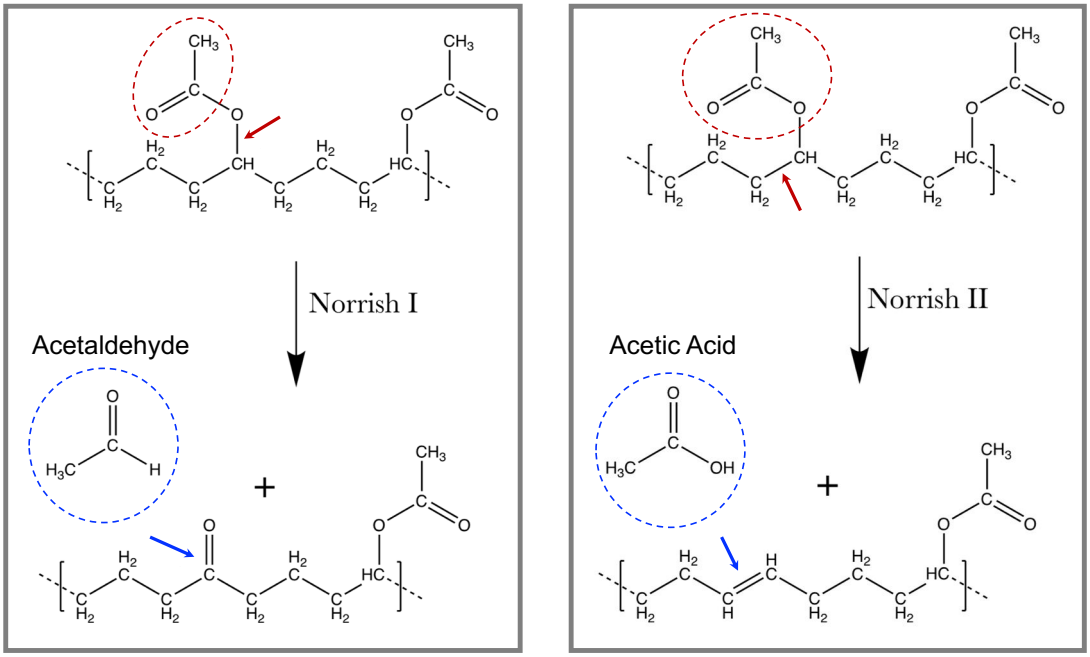

Fig. 3 Products of EVA deacetylation following the Norrish I and Norrish II mechanisms. EVA is represented using the polymer repeat unit –[CH_2-CH_2-CH_2-CH(-O-CO-CH_3)]$_2$– and in the product polymers, one of the acetate units has cleaved off to form acetaldehyde or acetic acid. Red arrows and circles represent the cleaved bond and chemical block respectively in EVA, while blue arrows and circles represent the new bond and acetaldehyde/acetic acid, respectively.

was increased to simulate this infinitely repeating (in the z direction) cross-linked EVA that does not interact with adjoining cross-linked chains in the x or y directions. Several intermediate structures were created to map out the polymer decomposition process from the starting structure to the final structure as pictured for different cases in Fig. 4. These structures served as input to an NEB calculation, a standard first principles approach used to determine the minimum energy path and activation energy of chemical reactions and processes[16,17]. Spring forces are applied on each atom of any 'image' to nudge it closer to the lowest energy barrier pathway. The *energy barrier* of the reaction is defined using the maximum energy structure that is passed while transitioning between the starting and final structures. We performed NEB calculations for the Norrish I and Norrish II mechanisms in vacuum and in the presence of a uniform solvation environment to determine the effect of the solvent on deacetylation energy barrier. We further examined the effect of an OH^- catalyst on the energy barrier by comparing the Norrish II mechanism with and without the catalyst. Finally, we studied the effect of the percentage of deacetylation on the energy barrier by performing the Norrish II NEB calculations for EVA with one formula unit and EVA with two formula units. We compared the computed energy barriers with experimentally reported activation energies and make statements on the most likely mechanisms and products of the decomposition process.

3 Results and Discussion

There are multiple reports in the literature on degradation of EVA quantified in terms of discoloration, loss of acetic acid and activation energies[14,27,28]. In their review paper, Czanderna et al.[19] cover various possible EVA decomposition mechanisms, their characterization and activation energies, and report that acetic acid and acetaldehyde are products of EVA degradation that further catalyze the degradation process. An experimental study by Pern et al.[27] reports that the hydrolysis-driven deacetylation of EVA with a 33% vinyl acetate content leads to the formation of acetic acid and the presence of either a vinyl alcohol group or a C=C double bond in the polymer chain, with an observed activation energy of 0.93 eV. Another experimental study by Rimez et al.[28] reports a higher activation energy of 1.97 eV and the presence of acetic acid and a C=C double bond in the polymer backbone, but with a 60–73% vinyl acetate content. Further, a DFT study of the degradation of an EVA-vinyl alcohol system with one transition state by Letant et al.[14] showed an energy barrier of 1.37 eV. In this section, we present in detail our NEB calculated reaction pathways, transition states, and energy barriers for Norrish I and Norrish II mechanisms, with and without catalyst, with and without solvent, for different percentages of deacetylation, and compare our results with the literature.

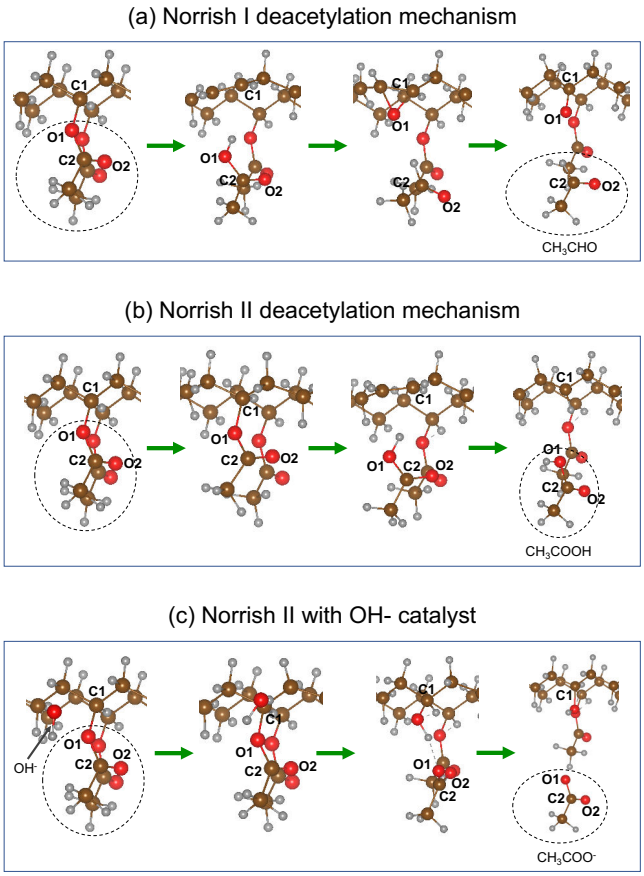

Fig. 4 Deacetylation reaction mechanisms captured via starting, intermediate and final structures (in clockwise direction) for (a) Norrish I, (b) Norrish II without catalyst, and (c) Norrish II with an OH^- catalyst.

3.1 Norrish II has lower energy barriers than Norrish I mechanism

The general deacetylation mechanisms for Norrish I and Norrish II without the presence of a catalyst are captured in Fig. 3. The essential reaction process involves the gradual loss of the acetate unit from the EVA polymer backbone and the rearrangement of the polymer chain to form either a new C=C double or a C=O ketone linkage. The amount of deacetylation can be estimated by measuring the acetaldehyde or acetic acid released as a result, as has been common practice[19]. We modeled the two mechanisms by creating 5 intermediate images (structure 1, 2, 3, 4, 5) between the starting and final structures and letting the NEB algorithm optimize the images so as to place each of them as transition states in the lowest energy pathway going from structure 0 (starting) to structure 6 (final). The starting and final structures along with two intermediate structures as modeled for different mechanisms in this work are pictured in Fig. 4. The EVA molecular structures shown in Fig. 4 represent the one formula unit (f.u.) renditions of EVA, and will be distinguished from the two f.u. renditions when discussing the effect of % of deacetylation on the energy barrier.

In Fig. 5, the NEB computed structure image energy as a function of the reaction coordinate is plotted for different cases, namely the Norrish I mechanism for one f.u. EVA with no catalyst (a), the Norrish II mechanism for one f.u. EVA with no catalyst (b), the Norrish II mechanism for one f.u. EVA with an OH^- catalyst (c), and the Norrish II mechanism for two f.u. EVA with no catalyst (d). It can be seen from Fig. 5 (a) and (b) that the highest energy points for both Norrish I and Norrish II mechanisms on one f.u. EVA occur around structure 4 or 5. The Norrish I energy barrier is computed to be 1.88 eV in vacuum and is reduced to 1.74 eV in a uniform solvation environment which is simulated using VASPsol[24]. In comparison, the Norrish II energy barriers are much lower at 0.86 eV in vacuum and 0.61 eV in solvent, showing that there is a clear energetic preference for deacetylation occurring via the Norrish II mechanism leading to the formation of acetic acid. This is consistent with multiple reports in the literature where acetic acid is detected in Si PV modules with EVA encapsulants[19] and used to quantify the degree of EVA decomposition. It is also notable that the energy barriers for both Norrish I and II mechanisms are reduced by the presence of a solvent, which implies that a moisture-driven Norrish II deacetylation process leading to acetic acid formation is the most energetically likely process.

3.2 Effect of Catalyst in Norrish II Mechanism

The presence of moisture in Si modules is likely to affect the polymer encapsulant decomposition, and it could be in terms of catalyzing the reaction via ions such as H^+, OH^- or H_3O^+. To study this effect, we modeled the hydrolysis-driven deacetylation of EVA via a pseudo- Norrish II mechanism using an OH^- catalyst that attacks the polymer backbone and facilitates the acetate unit cleavage, as seen in Fig. 4 (c). In this particular case, the products were the acetate anion (CH_3-CO-O^-) and a polymer with a vinyl alcohol (-OH) functional group where the acetate used to be. Upon modeling this hydrolysis reaction using NEB, we discovered that the energy barriers for Norrish II are indeed significantly reduced. As plotted in Fig. 5 (c), it can be seen that hydrolysis in vacuum shows an energy barrier of 0.57 eV, which is lower than the energy barrier of 0.86 eV for the Norrish II mechanism without catalyst. Similarly, in a solvation environment, the hydrolysis mechanism showed a reduced barrier of 0.31 eV as compared to 0.61 eV without catalyst. These observations support the experimental thesis of increased EVA degradation and acetic acid loss in the presence of moisture [refs]. Hydrolysis can be regarded as the major source of EVA deacetylation, and it can be stated that eliminating water in Si modules can go a long way towards retarding EVA decomposition. We also performed NEB computations for Norrish II deacetlyation using a potential H^+ catalyst, but observed much higher energy barriers which indicates that H^+ does not act as a catalyst unlike OH^-.

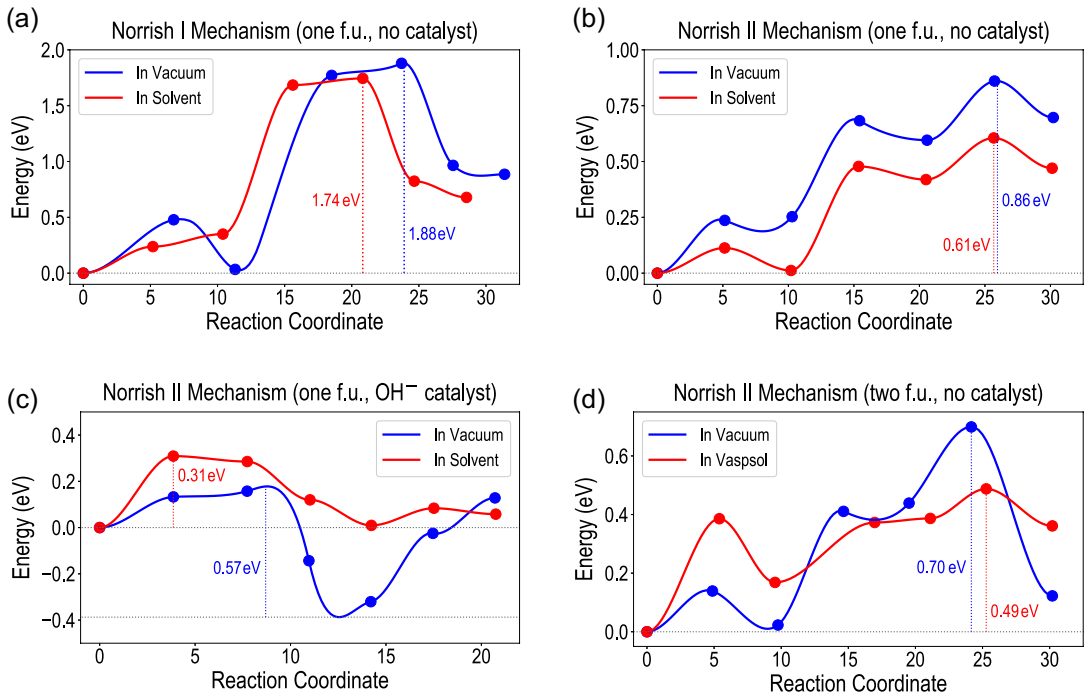

Fig. 5 NEB computed minimum energy pathways for EVA deacetylation mechanisms, including Norrish I (a) and Norrish II (b) on one f.u. EVA, Norrish II with an OH- catalyst on one f.u. EVA (c), and Norrish II on two f.u. EVA (d).

3.3 Effect of Percentage of Deacetylation in Norrish II Mechanism

While studying the process computationally, it is reasonable to model different degrees of deacetylation by using starting EVA structures with varying formula units. We investigated the effect of the percentage of deacetylation on the energy barrier by performing NEB calculations for the Norrish II mechanism on two EVA structures: one f.u.., which is what we call the systems pictured in Fig. 4, and two f.u., where we double the size of the system along the polymer chain direction and cleave one acetate unit off, reducing the percentage of deacetylation from 25% to 12.5%. As can be seen by comparing the NEB results in Fig. 5 (d) to the results in Fig. 5 (b), there is indeed an effect of how much acetate is being removed from the polymer repeat unit: the deacetylation energy barrier is reduced for the two f.u. case compared to one f.u., from 0.86 eV to 0.70 eV in vacuum and from 0.61 eV to 0.49 eV in the presence of solvent. While we use the one f.u. system for comparisons between the Norrish I and Norrish II mechanisms, and to illustrate the effect of a catalyst, the two f.u. Norrish II results are included when making comparisons of computer barriers with the experimental literature.

Our observation of a reduction in deacetylation energy barrier for a lower percentage of deacetylation is consistent with Rimez et al.[28] reporting an activation energy of 1.97 eV with a higher than typical vinyl acetate content of 60–73%. The range of deacetylation energy barriers in the literature, from 0.9 eV to 2 eV, is similar to some of the computed barriers in this work but differ quite a bit from the lower values in the presence of a catalyst. Overall, the computations are in qualitative agreement when considering the variable effects of external conditions like temperature, light and moisture, the chemical composition of EVA, addition of certain adhesion promoters like siloxane, etc., in the literature.

3.4 Computed IR Spectra of EVA and Decomposition Products

We performed DFPT computations on every optimized EVA and decomposition product structure and determined the IR intensities as a function of the wavenumber, which are plotted for all relevant systems in Fig. 6. DFPT computations have been successfully used in the past to determine and validate experimentally measured FTIR spectra of polymers, as well as to attribute certain frequencies to stretching, rotation or wagging modes[9–11]. From DFPT, the IR intensities of the characteristic modes of vibration in a material are obtained as a byproduct of the calculation of the ionic component of the dielectric constant using dynamical matrices and Born effective charges[23]. Plotted in this figure are computed IR spectra for all single chain, crystalline and cross-linked structures of EVA (red bars in the top half of Fig. 6(a)) and degradation product polymers (blue bars in top half of Fig. 6(b)), both in the presence of water (green bars in top half of Fig. 6(b)) and dry condition. The EVA structures used for these calculations in the presence of a water molecule are pictured in Fig. 2, while the degradation product polymers are pictured at the end of the clockwise loops in Fig. 4. We also measured the FTIR spectra of

dry and previously soaked EVA samples, and present this data in the bottom halves of the two plots in Fig. 6. EVA samples were fabricated by laminating 3M EVA9100 film between two teflon sheets under typical solar module lamination conditions. The dry sample was measured as fabricated, while the soaked sample was submerged in a 75°C water bath for 4 hours and subsequently allowed to dry out at room condition prior to measurement.

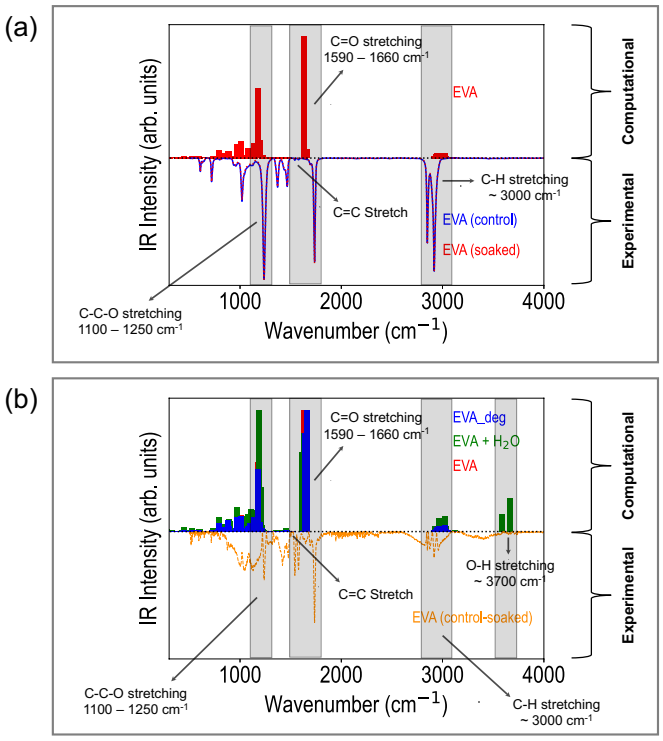

Fig. 6 Computed IR spectra for various crystalline and cross-linked structures of EVA and decomposition products (top half), compared with measured spectra (bottom half). The dry (control) and soaked samples of EVA are pictured in blue and red respectively. The computed spectra for the EVA structures are shown in (a) in red, while the computed spectra for EVA degradation products (in blue) and EVA structures with added water (in red) are shown in addition in (b).

We find that across all the structures used for EVA and degradation products, the prominent modes of vibration appear in approximately the same wavelength ranges as reported in the literature[14,29]. Such modes include C=O stretching (1590–1660 cm^{-1}), C-C-O stretching (1100–1250 cm^{-1}), C-H stretching (~ 3000 cm^{-1}) and O-H stretching (3600–3750 cm^{-1}, when there is a water molecule in the structure). We also find the C=O, C-C-O and C-H stretching modes occurring at similar wavenumbers in the experimental FTIR spectra. The wavenumber ranges for these modes have been marked using shaded grey bars that not only show the computed and measured peaks roughly coinciding, but also help capture the inherent uncertainties in DFPT computations which make them accurate only in a range rather than specific wavenumber values. In Fig. 6(b), the experimental spectra is represented as a difference in intensities between the control and soaked samples, magnified to highlight the key changes. Consequential mode differences can be seen in both the C-C-O and C=O stretching regions, while some additional modes of vibration appear in the 1590–1660 cm^{-1} range which are hypothesized to correspond to the stretching of the C=C double bond that forms in the polymer backbone as a result of EVA deacetylation following the Norrish II mechanism, as shown in Fig. 3.

There is a good qualitative match in the wavenumber ranges for C-C-O stretching, C=O stretching and C-H stretching computed and measured in this work and the FTIR spectra reported by Sigma Aldrich [ref]. The O-H stretching modes appear from the presence of a water molecule in the system, modeled for each EVA structure as shown in Fig. 2: this enables the characterization of moisture in EVA and its decomposition products. While the presence of O-H stretching modes in the ~ 3700 cm^{-1} range can help illustrate the presence of water, it can be seen that the various structures being studied here cannot necessarily be distinguished in terms of the C-C-O, C=O or C-H stretching modes. The appearance of a subtle C=C stretching mode, as explained in the previous paragraph, can help ascertain, along with the presence of acetic acid, the occurrence of the Norrish II deacetylation mechanism.

4 Conclusions

In summary, we performed density functional theory computations to study the atomistic structures, decomposition mechanisms and IR spectra of ethylene vinyl acetate (EVA), the most common polymer used as encapsulant in Si PV modules. The computational results provide justification for experimentally observed phenomena and illustrate possible ways to limit the de-adhesion or delamination process in Si modules. We optimized the structures of EVA in single chain, crystalline and cross-linked forms, and used single chain versions of the cross-linked structure to model deacetylation reaction mechanisms via several intermediate or transition state structures. The nudged elastic band (NEB) method was applied to calculate minimum energy pathways for various mechanisms and the computed energy barriers revealed that the Norrish II mechanism of acetic acid formation is more favorable than the Norrish I mechanism leading to acetaldehyde formation. The Norrish II mechanism is further brought down by a hydrolysis-driven reaction catalyzed by a hydroxyl (OH^-) ion, as well as by reducing the amount of acetate group loss from 25% to 12.5%. The computed IR active modes for EVA and deacetylation products with and without water match qualitatively well with measured spectra from our laboratory experiments and from available literature. The detection of "additional" modes of vibration corresponding to O-H or C=C stretching can help ascertain the presence of moisture or the occurrence of the Norrish II deacetylation mechanism. The computational studies performed in this work can be extended for other polymer encapsulants of interest such as polyolefins, and extended to include the effects of metallic contacts, dielectric layers, and various relevant interfaces which are important components of the Si PV module.

Conflicts of interest

There are no conflicts to declare.

Acknowledgements

This material is based upon work supported by the U.S. Department of Energy's Office of Energy Efficiency and Renewable Energy (EERE) under Solar Energy Technologies Office (SETO) Agreement Number DE-EE0008160. Use of the Center for Nanoscale Materials, an Office of Science user facility, was supported by the U.S. Department of Energy, Office of Science, Office of Basic Energy Sciences, under Contract No. DE-AC02-06CH11357. This research used resources of the National Energy Research Scientific Computing Center (NERSC), a DOE Office of Science User Facility supported by the Office of Science of the U.S. Department of Energy under Contract No. DE-AC02-05CH11231. The DFT computations were performed and analyzed by A.M.K. and M.K.Y.C. using the high-performance computing clusters operated by the Laboratory Computing Resource Center (LCRC) and the Center for Nanoscale Materials (CNM) at Argonne National Laboratory, as well as the resources from NERSC at Berkeley Lab. Experimental measurements were conducted by R.E.K. and D.P.F.

References

1 Y. Xu, R. He and F. Jin, *IOP Conference Series: Materials Science and Engineering*, 2018, **452**, 032105.

2 A. Rehman and S. Lee, *Materials*, 2014, 1318 – 1341.

3 J.-F. Lelièvre, E. Fourmond, A. Kaminski, O. Palais, D. Ballutaud and M. Lemiti, *Solar Energy Materials and Solar Cells*, 2009, **93**, 1281 – 1289.

4 M. C. C. de Oliveira, A. S. A. D. Cardoso, M. M. Viana and V. de Freitas Cunha Lins, *Renewable and Sustainable Energy Reviews*, 2018, **81**, 2299 – 2317.

5 D. Wu, J. Zhu, T. R. Betts and R. Gottschalg, *Progress in Photovoltaics: Research and Applications*, 2014, **22**, 796–809.

6 R. E. Kumar, G. v. Gastrow, J. Leslie, R. Meier, M. I. Bertoni and D. P. Fenning, *IEEE Journal of Photovoltaics*, 2019, **9**, 1748–1753.

7 A. Mannodi-Kanakkithodi, G. M. Treich, T. D. Huan, R. Ma, M. Tefferi, Y. Cao, G. A. Sotzing and R. Ramprasad, *Advanced Materials*, 2016, **28**, 6277–6291.

8 A. Mannodi-Kanakkithodi, G. Pilania, T. D. Huan, T. Lookman and R. Ramprasad, *Scientific Reports*, 2016, **6**,.

9 V. Sharma, C. Wang, R. G. Lorenzini, R. Ma, Q. Zhu, D. W. Sinkovits, G. Pilania, A. R. Oganov, S. Kumar, G. A. Sotzing, S. A. Boggs and R. Ramprasad, *Nature Communications*, 2014, **5**,.

10 T. D. Huan, A. Mannodi-Kanakkithodi, C. Kim, V. Sharma, G. Pilania and R. Ramprasad, *Scientific Data*, 2016, **3**,.

11 A. F. Baldwin, R. Ma, A. Mannodi-Kanakkithodi, T. D. Huan, C. Wang, M. Tefferi, J. E. Marszalek, M. Cakmak, Y. Cao, R. Ramprasad and G. A. Sotzing, *Advanced Materials*, 2015, **27**, 346–351.

12 M. A. Matin, R. K. Chitumalla, M. Lim, X. Gao and J. Jang, *The Journal of Physical Chemistry B*, 2015, **119**, 5496–5504.

13 A. Prestianni, F. Ferrante, E. M. Sulman and D. Duca, *The Journal of Physical Chemistry C*, 2014, **118**, 21006–21013.

14 S. E. Letant, D. F. Plant, T. S. Wilson, C. T. Alviso, M. S. Read and R. S. Maxwell, *Polymer Degradation and Stability*, 2011, **96**, 2019 – 2028.

15 M. Blaško, P. Mach, A. Antušek and M. Urban, *The Journal of Physical Chemistry A*, 2018, **122**, 1496–1503.

16 G. Henkelman, B. P. Uberuaga and H. Jónsson, *The Journal of Chemical Physics*, 2000, **113**, 9901–9904.

17 D. Sheppard, R. Terrell and G. Henkelman, *The Journal of Chemical Physics*, 2008, **128**, 134106.

18 B. Marchetti, T. N. V. Karsili and M. N. R. Ashfold, *Phys. Chem. Chem. Phys.*, 2019, **21**, 14418–14428.

19 A. Czanderna and F. Pern, *Solar Energy Materials and Solar Cells*, 1996, **43**, 101 – 181.

20 K. Lee, E. D. Murray, L. Kong, B. I. Lundqvist and D. C. Langreth, *Phys. Rev. B*, 2010, **82**, 081101.

21 S. Goedecker, *The Journal of Chemical Physics*, 2004, **120**, 9911–9917.

22 M. Amsler and S. Goedecker, *The Journal of Chemical Physics*, 2010, **133**, 224104.

23 S. Baroni, S. de Gironcoli, A. Dal Corso and P. Giannozzi, *Rev. Mod. Phys.*, 2001, **73**, 515–562.

24 K. Mathew, R. Sundararaman, K. Letchworth-Weaver, T. A. Arias and R. G. Hennig, *The Journal of Chemical Physics*, 2014, **140**, 084106.

25 Z. Xia, D. W. Cunningham and J. H. Wohlgemuth, 2009 34th IEEE Photovoltaic Specialists Conference (PVSC), 2009, pp. 000124–000126.

26 C. Hirschl, M. Biebl–Rydlo, M. DeBiasio, W. Mühleisen, L. Neumaier, W. Scherf, G. Oreski, G. Eder, B. Chernev, W. Schwab and M. Kraft, *Solar Energy Materials and Solar Cells*, 2013, **116**, 203 – 218.

27 F. Pern and A. Czanderna, *Solar Energy Materials and Solar Cells*, 1992, **25**, 3 – 23.

28 B. Rimez, H. Rahier, G. V. Assche, T. Artoos, M. Biesemans and B. V. Mele, *Polymer Degradation and Stability*, 2008, **93**, 800 – 810.

29 J. K. Haken and R. L. Werner, *British Polymer Journal*, 1971, **3**, 157–162.